J. Micromech. Microeng. **14** (2004) 597–603 PII: S0960-1317(04)72108-7

A tapered hollow metallic microneedle array using backside exposure of SU-8

Kabseog Kim[1], Daniel S Park[1], Hong M Lu[1], Wooseong Che[2], Kyunghwan Kim[3], Jeong-Bong Lee[1] and Chong H Ahn[4]

[1] Erik Jonsson School of Engineering and Computer Science, The University of Texas at Dallas, Richardson, TX 75083, USA
[2] School of Information Engineering, Tongmyung University of Information Technology, Busan, Korea
[3] Department of Electric and Information Engineering, Kyungwon University, Seongnam, Korea
[4] Department of Electrical Engineering and Computer Science, University of Cincinnati, Cincinnati, OH 45221, USA

E-mail: kskim@utdallas.edu

Received 18 November 2003
Published 6 February 2004
Online at stacks.iop.org/JMM/14/597 (DOI: 10.1088/0960-1317/14/4/021)

Abstract
This paper presents a novel fabrication process for a tapered hollow metallic microneedle array using backside exposure of SU-8, and analytic solutions of critical buckling of a tapered hollow microneedle. An SU-8 mesa was formed on a Pyrex glass substrate and another SU-8 layer, which was spun on top of the SU-8 mesa, was exposed through the backside of the glass substrate. An array of SU-8 tapered pillar structures, with angles in the range of 3.1°–5°, was formed on top of the SU-8 mesa. Conformal electrodeposition of metal was carried out followed by a mechanical polishing using a planarizing polymeric layer. All organic layers were then removed to create a metallic hollow microneedle array with a fluidic reservoir on the backside. Both 200 μm and 400 μm tall, 10 by 10 arrays of metallic microneedles with inner diameters of the tip in the range of 33.6–101 μm and wall thickness of 10–20 μm were fabricated. Analytic solutions of the critical buckling of arbitrary-angled truncated cone-shaped columns are also presented. It was found that a single 400 μm tall hollow cylindrical microneedle made of electroplated nickel with a wall thickness of 20 μm, a tapered angle of 3.08° and a tip inner diameter of 33.6 μm has a critical buckling force of 1.8 N. This analytic solution can be used for square or rectangular cross-sectioned column structures with proper modifications.

1. Introduction

Hypodermic syringes with a hollow pointed needle have been one of the most commonly used body fluid extraction, vaccination and medication devices since their insertion by Pravaz and Wood back in the 1850s [1]. While there have been many variations in materials and methods of providing safety, hypodermic syringe design itself has changed very little from its first use. Conventional hypodermic needles create fear of injection-related pain among patients and there has been increasing concern about the risks of transmitting blood born pathogens such as HIV (human immunodeficiency virus) or hepatitis to health-care workers by accidental needle stick injuries [2]. In the US alone, approximately one million needle stick injuries are reported annually.

Recently, there have been many investigations on the development of alternative designs of hypodermic needles with a goal of creating safer and minimally invasive transdermal drug delivery and body fluid sampling devices. Mitragotri *et al* [3] used low-frequency ultrasound to increase the permeability of human skin by several orders of magnitude compared to the case without ultrasound activation and demonstrated transdermal delivery of high molecular weight proteins such as insulin, interferon gamma and erythropoeitin.

Such research opened the possibility of creating a needleless transdermal drug delivery device. Henry *et al* [4] used silicon micromachining techniques to create an array of sharp solid silicon microstructures with a height of 150 μm and used such microstructures as a microneedle array to demonstrate increased permeability of human skin by up to four orders of magnitude *in vitro*. Such structural height ensures that the microneedle array penetrates just beneath the viable epidermis resulting in efficient drug delivery with minimal pain. McAllister *et al* [5] demonstrated both tapered-shaft and straight-shaft hollow metallic microneedle arrays for transdermal drug delivery applications and microcombustion applications. Lin and Pisano [6] demonstrated 1, 3 and 6 mm long single hollow silicon hypodermic microneedles with fully enclosed fluidic channels. Since it is CMOS compatible, it has a great possibility of integration with electronics to realize smart microneedles. Chandrasekaran and Frazier [7] also demonstrated single hollow metallic hypodermic microneedles and their arrays using electroplated palladium, palladium alloys and nickel.

Microneedles and microneedle arrays can be used as stand-alone devices as well as parts of a more complicated biological detection/delivery system. Zimmermann *et al* [8] demonstrated a disposable self-calibrating continuous glucose monitor using hollow microneedles with a porous poly-Si dialysis membrane and enzyme-based flow-through sensor. Ahn *et al* [9] demonstrated a point-of-care clinical diagnostic system using multiple stacks of disposable functional plastic bio chips with microneedles as body fluid sampling devices.

The goal of this paper is two-fold. First, we report a new fabrication method of a tapered hollow metallic microneedle array. The novel method is based on the backside exposure of a double layer of SU-8 through a glass substrate. The fabrication process is low cost, mass production compatible, and is simple and straightforward compared to previous approaches. Second, we report an extended analytic solution of the critical buckling of the microneedle structures. The analytic solutions of the critical buckling used in microneedle research were primarily based on a model of fixed–free prismatic columns although the real structures are typically tapered hollow columns. This paper presents an extended analytic solution of critical buckling of fixed–free truncated cone column structures. Such analytic solutions can be used to determine the critical buckling of hollow microneedles.

2. Backside exposure of SU-8

SU-8-based UV-LIGA processes are commonly used to create very thick, high aspect ratio polymeric and/or metallic microstructures. The thicker the resist structures, the larger the difference between the UV exposure dose at the top of the resist and the bottom of the resist. Due to such non-uniform UV exposure dose, typically the top layer is overexposed and the bottom layer is relatively underexposed resulting in the variation of the lateral dimensions of the developed resist structures at the top and at the bottom. Since SU-8 is an epoxy-based negative-tone resist, the top structure tends to be wider than the structures at the bottom of SU-8. It is a particularly significant problem when SU-8 is used for creating metallic mold structures. Recently, Peterman *et al* [10] suggested a backside exposure of thick SU-8 through a mask defined on a glass substrate to create a reentrant SU-8 structure for easy metallic mold production.

In this work, we used backside exposure of double-layered SU-8 through a Pyrex 7740 glass substrate. Tapered SU-8 pillar array structures were thus created using a conventional UV mask and contact printing method. A mask was designed to have circular geometry with diameters of 40, 60, 80 and 100 μm. Figure 1 shows the process sequence of the backside exposure of double-layered SU-8. The experiment was started with a spin-coating of an SU-8 release layer on top of a 3 inch diameter, 700 μm thick Pyrex 7740 glass substrate. A layer of 200 μm thick SU-8 2075 was spin-coated and was left on a flat surface for an hour for stress relaxation. The SU-8 was then baked at 65 °C for 5 min and at 95 °C for 45 min on a hotplate. UV exposure was carried out with a dose of 1000 mJ cm^{-2} and a post-exposure bake was performed at 65 °C for 1 min and 95 °C for 15 min (figure 1(*a*)). Another 200 μm thick layer of SU-8 was spin-coated on top of the post-exposure-baked first SU-8 layer (figure 1(*b*)). The double-layered SU-8 was soft-baked and exposed to the UV light with two different doses: 1000 mJ cm^{-2} and 1500 mJ cm^{-2} (figure 1(*c*)). The samples were then developed in a SU-8 developer for approximately 90 min and cleaned in an oxygen plasma (200 W, 100% O_2) for about 2 min using a reactive ion etcher (figure 1(*d*)). Figure 2 shows the fabrication results of such backside exposed double-layered SU-8 structures. Figure 2(*a*) shows the result with a dose of 1000 mJ cm^{-2} and figure 2(*b*) shows the result with a dose of 1500 mJ cm^{-2}. With a 1000 mJ cm^{-2} dose, the sidewall of the SU-8 pillar structures was relatively rough due to an insufficient exposure dose. With an increased exposure dose (1500 mJ cm^{-2}), the sidewall of the SU-8 pillar structures turned out to be fairly smooth (figure 2(*b*)) and a decent tapered SU-8 pillar structure was formed. An array of SU-8 pillar structures 400 μm in height was also developed with a dose of 2500 mJ cm^{-2}. Table 1 shows the measured top and bottom diameters and angles of the 200 μm and 400 μm tall tapered SU-8 pillar structures. For the 200 μm tall SU-8 pillars, angles in the range of 4.37°–5° were realized with top diameters in the range of 38–101 μm. For the 400 μm tall SU-8 pillars, angles in the range of 3.08°–4.48° were realized with top diameters in the range of 33.6–91.4 μm. It can be noted that 400 μm tall SU-8 pillars have smaller dimensions at the top and larger dimensions at the bottom compared to those of 200 μm tall SU-8 pillars. This is due to larger uneven exposure dose distribution through the thicker SU-8.

3. Fabrication of a hollow metallic microneedle array

Based on the double-layered SU-8 backside exposure results, tapered hollow metallic microneedle arrays were fabricated. Figure 3 shows the fabrication sequence and figure 4 shows a series of SEM photomicrographs of the microneedle array fabrication. A double-layer (100 Å chromium and 1000 Å copper) electroplating seed was conformally deposited on top of the patterned double-layered SU-8 pillar array structures (figure 3(*a*)). Nickel electroplating was carried out using a nickel sulfamate bath ($(Ni(SO_3.NH_2))_2$ 82 g, H_3BO_3 37.5 g and

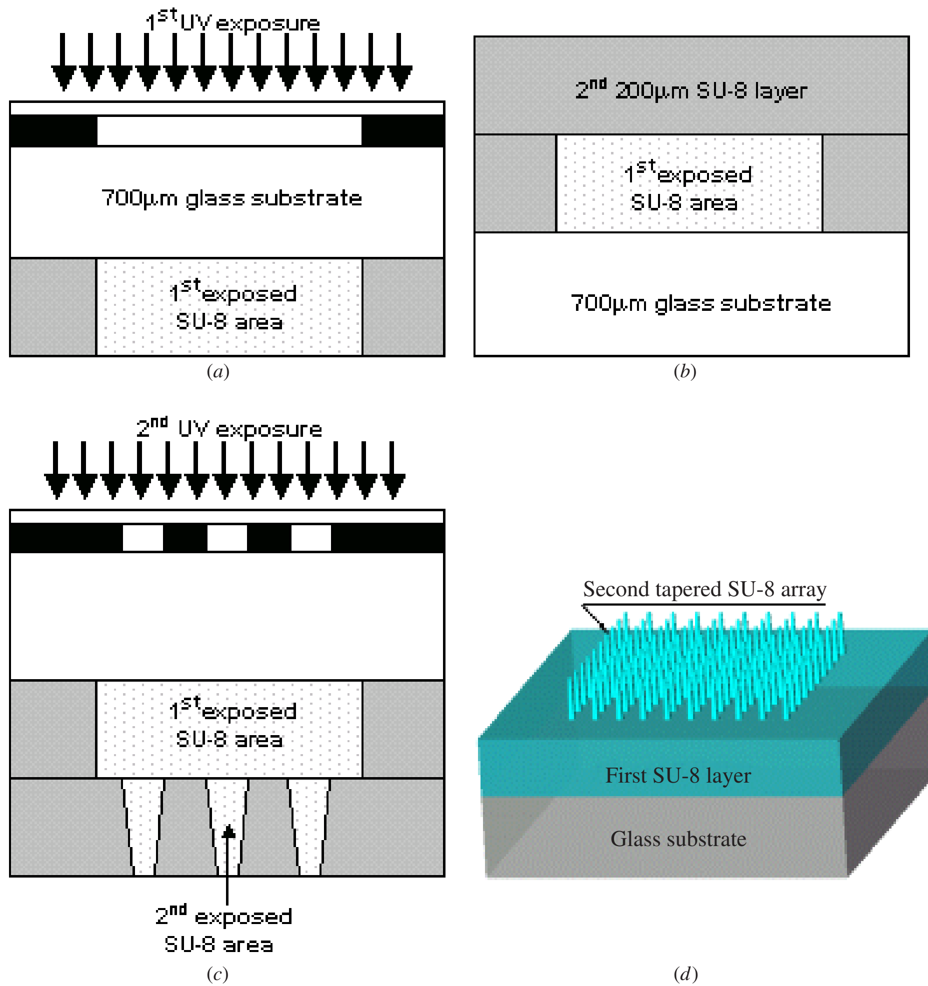

Figure 1. A schematic of the process flow to fabricate tapered SU-8 pillar structures: (*a*) first 200 μm thick SU-8 exposure through a glass substrate, (*b*) second 200 μm thick SU-8 layer preparation, (*c*) the second SU-8 layer exposure through the glass substrate and the exposed first SU-8 layer to create an array of tapered SU-8 structures and (*d*) a general view of the fabricated double-layered SU-8 on a glass substrate.

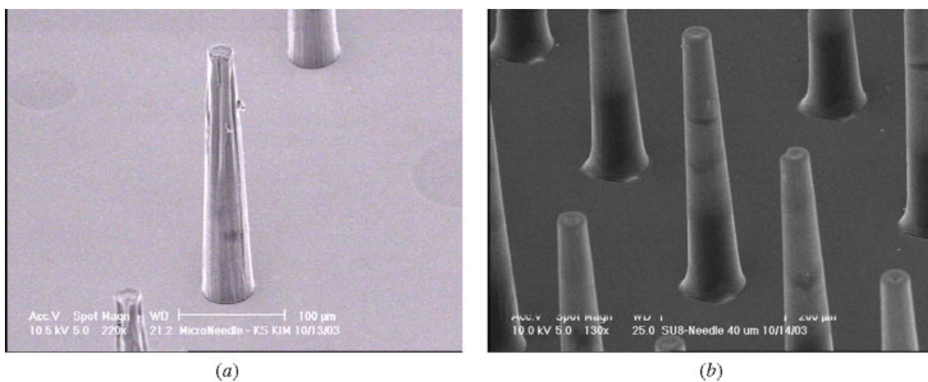

Figure 2. SEM photomicrographs of 200 μm SU-8 pillar arrays processed at the different UV doses: (*a*) 1000 mJ cm^{-2} and (*b*) 1500 mJ cm^{-2}.

lauryl sulfate 3 g in 1 liter of de-ionized water) at 55 °C with a current density of 5 mA cm^{-2} (figure 3(*b*)). Figure 4(*a*) shows the SEM photomicrograph of a 400 μm tall tapered SU-8 pillar structure and figure 4(*b*) shows the same after the nickel electroplating. In order to open the tips of the microneedle array, an additional 450 μm thick SU-8 layer was blanket deposited to provide an organic planarizing layer (figure 3(*c*)). The SU-8 layer was soft-baked and mechanically polished until the microneedle tips were opened (figure 3(*d*)) and the unexposed planarizing SU-8 layer was removed by dipping in a developer. Figure 4(*c*) shows the SEM photomicrograph of the top view of the opened tip of a microneedle. Next, the SU-8 release layer was stripped off resulting in the separation of electrodeposited nickel coated double-layered SU-8 pillar

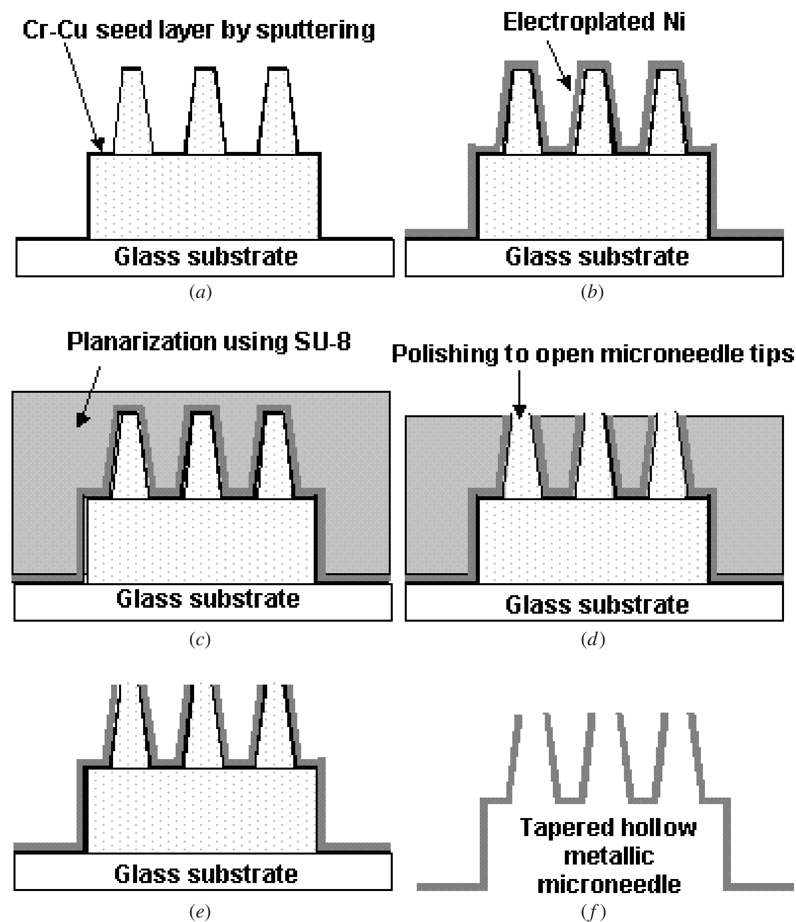

Figure 3. A schematic of the process flow to fabricate a tapered metallic hollow microneedle array: (*a*) 100 Å Cr and 1000 Å Cu seed layer deposition by sputtering, (*b*) nickel electroplating, (*c*) planarizing SU-8, (*d*) polishing to open the microneedle tip, (*e*) removal of SU-8 planarization layer and separation of the microneedle array from the glass substrate and (*f*) removal of SU-8.

Table 1. Measured dimensions of the 200 μm and 400 μm SU-8 pillar structures.

Diameters on the mask	Diameters on SU-8 pillars					
	200 μm tall SU-8 pillar			400 μm tall SU-8 pillar		
	Bottom	Top	Angle	Bottom	Top	Angle
40 μm	72.6 μm	38.0 μm	4.94°	76.7 μm	33.6 μm	3.08°
60 μm	95.8 μm	65.2 μm	4.37°	115 μm	58.2 μm	4.06°
80 μm	114 μm	81.3 μm	4.67°	137 μm	74.3 μm	4.48°
100 μm	136 μm	101 μm	5.0°	150 μm	91.4 μm	4.19°

structures from the glass substrate (figure 3(*e*)). Finally, the double-layered SU-8 structures were dry etched using O_2/CF_4 (80%:20%) plasma with a power of 500 W using a microwave plasma etch. It was followed by a wet etch of the electroplating seed layer resulting in a tapered hollow metallic microneedle array with a fluidic reservoir on the backside (figure 3(*f*)). Figures 4(*d*) and (*e*) show SEM photomicrographs of the 200 μm and 400 μm tall hollow metallic microneedle arrays from the top side. The metallic wall thickness for the 200 μm tall microneedle is 10 μm and that for the 400 μm tall microneedle is 20 μm. Figure 5(*a*) shows a SEM photomicrograph of a 400 μm tall microneedle array with a conventional gauge 28 stainless steel needle and figure 5(*b*) shows the backside of the hollow microneedle array which shows the fluidic reservoir and holes defined by complete removal of SU-8.

4. Analytic solution of the critical buckling for a tapered hollow microneedle

A microneedle needs to be mechanically strong enough to penetrate the skin without mechanical failure. Two mechanical failure modes are of interest in this regard: critical buckling and yield failure. If such failures occur, a small piece of broken needle may be left inside the skin, which may cause biological complications. The yield failure occurs when a load greater than yield strength of the material is applied. The yield strength is an intrinsic material property independent

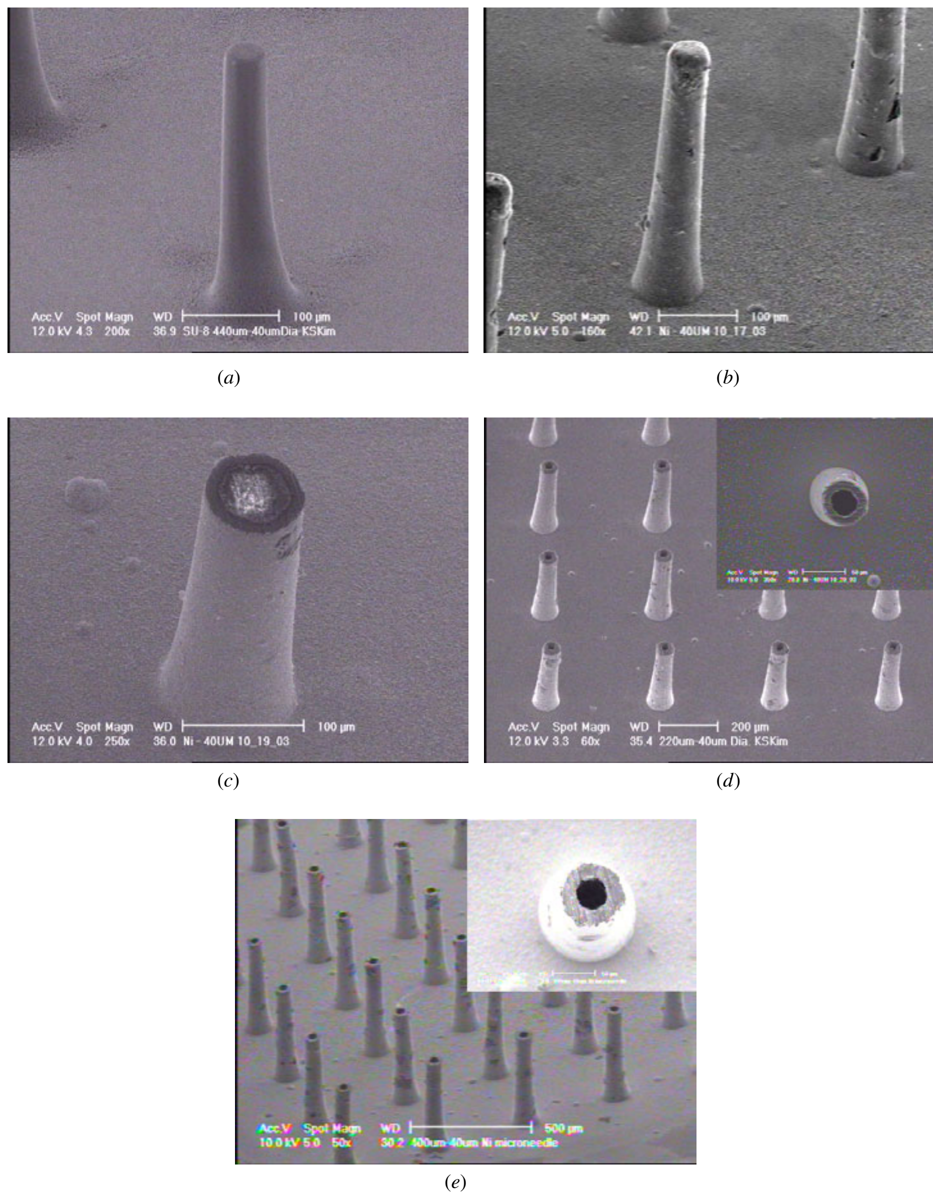

Figure 4. SEM photomicrographs of a microneedle array under fabrication: (*a*) 400 μm tall tapered SU-8 pillar, (*b*) electroplated nickel covered SU-8 pillar, (*c*) an opened microneedle tip after SU-8 planarization and polishing, (*d*) 200 μm tall metallic hollow microneedle array and (e) 400 μm tall metallic hollow microneedle array.

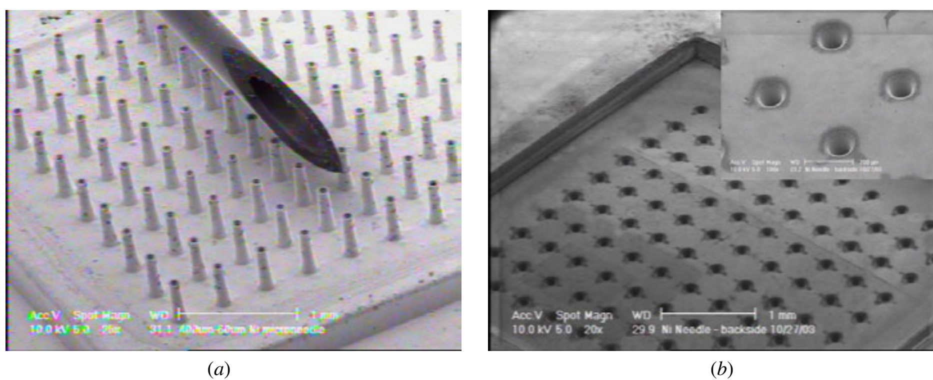

Figure 5. SEM photomicrographs of a microneedle array: (*a*) a 400 μm tall tapered hollow metallic microneedle array in comparison with a conventional stainless steel needle and (*b*) backside of the microneedle array which shows the fluidic reservoir and hollow holes.

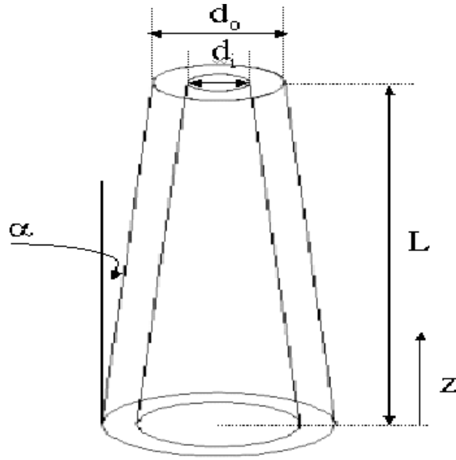

Figure 6. A schematic diagram of a hollow truncated cone column.

of mechanical geometry. Since microneedles are typically very high aspect ratio column-like structures, they are also susceptible to catastrophic buckling failure. Most previous work on microneedles used critical buckling of the fixed–free prismatic column even though they are fixed–free tapered hollow columns.

In this work, we derived analytic solutions for critical buckling of the fixed–free tapered hollow truncated cone column. Figure 6 shows a truncated cone column with a structural height L, a tapering angle α, an inner diameter d_i and an outer diameter d_o. The column is fixed at the bottom ($z = 0$) and is free at the top ($z = L$). In order to find the load that causes buckling of the column, one should solve the differential equation:

$$EI(z)\frac{\mathrm{d}^2 y(z)}{\mathrm{d}z^2} + M(z) = 0, \tag{1}$$

where E is Young's modulus of the material (assuming that it is homogeneous), $I(z)$ is the moment of inertia about the centroid, $y(z)$ is the assumed deflected shape, $M(z)$ is the bending moment. Smith [11] showed the critical buckling load (P_cr) of the fixed–free tapered column as

$$P_\mathrm{cr} = \frac{\pi^2 E}{2L^3}\int_0^L \sum_{i=0}^{n} k_i z^i \cos^2\left(\frac{\pi z}{2L}\right) \mathrm{d}z, \tag{2}$$

where $\sum k_i z^i = I(z)$ and k_i is the constant coefficient which is dependent on the column's cross section. Equation (2) can be applied to any columnar structure when area moment of inertia of arbitrary cross-sectional shape can be expressed by a polynomial of z. For the case of a hollow truncated cone column with an angle α, inner diameter d_i and an outer diameter d_o, the area moment of inertia at any position z is given by

$$I(z) = \frac{\pi}{64}\begin{bmatrix} \left(d_\mathrm{o}^4 - d_\mathrm{i}^4\right) + 8(L-z)\tan\alpha\left(d_\mathrm{o}^3 - d_\mathrm{i}^3\right) \\ +24(L-z)^2\tan\alpha^2\left(d_\mathrm{o}^2 - d_\mathrm{i}^2\right) \\ +32(L-z)^3\tan\alpha^3\left(d_\mathrm{o} - d_\mathrm{i}\right) \end{bmatrix}. \tag{3}$$

Then, the critical buckling load of the truncated hollow cone fixed–free column can be determined as follows:

$$P_\mathrm{cr} = \frac{E}{80\pi L^2} \times \begin{bmatrix} \frac{5\pi^4}{16}\left(d_\mathrm{o}^4 - d_\mathrm{i}^4\right) + \left(5\pi^2 + \frac{5}{4}\pi^4\right)\left(d_\mathrm{o}^3 - d_\mathrm{i}^3\right) L\tan\alpha \\ +\left(15\pi^2 + \frac{5}{2}\pi^4\right)\left(d_\mathrm{o}^2 - d_\mathrm{i}^2\right) L^2\tan\alpha^2 \\ +\left(-120 + 30\pi^2 + \frac{5}{2}\pi^4\right)\left(d_\mathrm{o} - d_\mathrm{i}\right) L^3\tan\alpha^3 \end{bmatrix}. \tag{4}$$

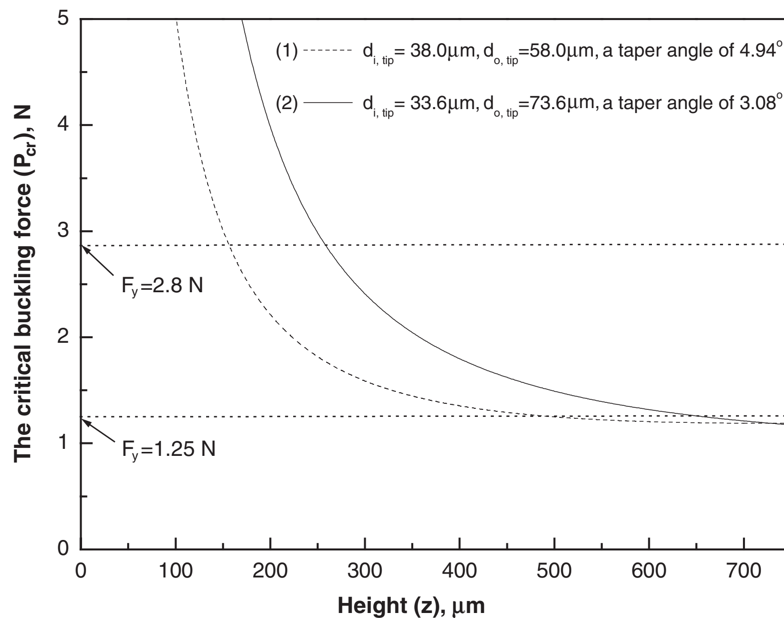

Figure 7. The critical buckling forces and the yield strength limits as a function of the height of microneedle for two different cases: (1) $d_\mathrm{i} = 38$ μm, $d_\mathrm{o} = 58$ μm, a taper angle of 4.94°, (2) $d_\mathrm{i} = 33.6$ μm, $d_\mathrm{o} = 73.6$ μm, a taper angle of 3.08°at the tip.

For a prismatic column with a diameter d, the critical buckling load becomes

$$P_{\mathrm{cr}} = \frac{E\pi^3 d^4}{256L^2} = \frac{\pi^2 EI}{4L^2}. \quad (5)$$

For a single 400 μm tall electroplated nickel microneedle with a tapered angle of 3.08°, a wall thickness of 20 μm and an inner diameter of the tip of 33.6 μm, the critical buckling force is found to be 1.8 N based on Young's modulus of the electroplated nickel of 23.1 GPa [12]. Based on the yield strength of 830 MPa [12], the force that reaches the yield strength at the tip of the electroplated nickel hollow microneedle is found to be 2.8 N. For a single 200 μm tall microneedle with a tapered angle of 4.94°, a wall thickness of 10 μm and an inner diameter of the tip of 38 μm, the critical buckling force is found to be 2.25 N and the force that reaches the yield strength at the tip is found to be 1.25 N. Figure 7 shows the critical buckling forces and the yield strength limits for single electroplated microneedles with dimensions of 200 μm tall (4.94°, 58 μm outer diameter, 38 μm inner diameter at the tip) and 400 μm tall (3.08°, 73.6 μm outer diameter, 33.6 μm inner diameter at the tip). Since our design has 10 by 10 array of microneedles, assuming the uniformly distributed external stress, both buckling force and yield strength limit will be 100 times greater than that of the single microneedle.

Although the critical buckling force is considered to be a critical parameter of the device design, since the deflection of the microneedle would not be small even with relatively small shear forces and/or eccentric axial loads, more likely causes of mechanical failure of microneedles would be either shear forces or eccentric axial loads. When these forces are considered, the maximum load should be determined by the maximum amount of the allowable deflection of the microneedle. When an eccentric axial load P (the axial load that is not perfectly along the axis) is applied to the microneedle, the maximum deflection at the tip (δ) is given by

$$\delta_{\max} = e\left(\sec\sqrt{\frac{P_{\max}}{EI}}L - 1\right), \quad (6)$$

where e is the eccentricity from the center of the axis. When a shear force (V) applies to the tip of the microneedle (assuming that the microneedle is a prismatic column), the maximum deflection at the tip is given by

$$\delta_{\max} = \frac{V_{\max} L^3}{3EI}. \quad (7)$$

This analytic solution can be used for other cross-sectional shaped columns (such as square or rectangular) with different expressions of the area moment of inertia. This analytic solution can be used for critical buckling analysis of various practical microneedles as well as other common columnar microstructures.

5. Conclusions

A 10 by 10 tapered hollow electroplated nickel microneedle array with a fluidic reservoir on the backside was realized by backside exposure of double-layered SU-8 through a glass substrate. Both 200 μm tall and 400 μm tall microneedles with tapering angles less than 5° degree were realized. Since this process is rapid, simple and relatively inexpensive in nature, it may be used in the manufacturing of commercial metallic microneedles for painless drug delivery and body fluid sampling. In order to realize metallic microneedles for clinical applications, fabrication methods using biocompatible metals should be studied.

In addition to the novel fabrication method development, an extended analytic solution of the critical buckling force of the fixed–free truncated cone column was derived. Such analytic solutions can be used for common microneedle structures. It can also be used for critical buckling analysis of various columnar structures with small modifications.

Acknowledgments

This work was supported in part by the Defense Advanced Research Project Agency (DARPA) under the grant F30602-00-1-0569. The support of University of Texas at Dallas clean room staff for the fabrication of devices is acknowledged. Valuable technical discussions with Dr M Tinker, A Nallani, Dr J-C. Lee, K Colinjivadi and B Pillans of UTD Micro/Nano Devices and Systems Laboratory and Y Desta of Louisiana State University are greatly appreciated.

References

[1] McGrew R and MeGrew M 1985 *Encyclopedia of Medical History* (New York: McGraw Hill)
[2] Jagger J, Hunt E H, Brand-Elnaggar J and Person R D 1988 Rates of needle-stick injury caused by various devices in a university hospital *New Engl. J. Med.* **319** 284–8
[3] Mitragotri S, Blankschtein D and Langer R 1995 Ultrasound-mediated transdermal protein delivery *Science* **269** 850–3
[4] Henry S, McAllister D V, Allen M G and Prausnitz M R 1998 Micromachined needles for transdermal delivery of drugs *Proc. 11th IEEE Int. Conf. MEMS* pp 494–8
[5] McAllister D V, Cros F, Davis S P, Matta L M, Prausnitz M R and Allen M G 1999 Three-dimensional hollow microneedle and microtube arrays *10th Int. Conf. Solid-State Sensors and Actuators* pp 1098–101
[6] Lin L and Pisano A P 1999 Silicon-processed microneedles *J. MEMS* **8** 78–84
[7] Chandrasekaran S and Frazier A B 2003 Characterization of surface micromachined metallic microneedles *J. MEMS* **12** 288–95
[8] Zimmermann S, Fienbork D, Stoeber B, Flounders A W and Liepmann D 2003 A microneedle-based glucose monitor: fabricated on a wafer-level using in-device enzyme immobilization *12th Int. Conf. Solid-State Sensors and Actuators* pp 99–102
[9] Ahn C, Choi J, Beaucage G, Nevin J, Lee J B, Puntambekar A and Lee J Y 2004 Disposable smart lab-on-a-chip for point-of-care clinical diagnostics *Proc. IEEE* **92** 154–73
[10] Peterman M C, Huie P, Bloom D M and Fishman H A 2003 Building thick photoresist structures from the bottom up *J. Micromech. Microeng.* **13** 380–2
[11] Smith W G 1988 Analytic solutions for tapered column buckling *Comput. Struct.* **28** 677–81
[12] Fritz T, Leuerer T, Krüger C, Mokwa W and Schnakenberg U 2000 Mechanical properties of electroplated nickel *Technical Digest of Micro Materials Micro Mat 2000: 3rd Int. Conf. and Exhibition (Berlin, Germany)* pp 752–5